RSC Advances

ARTICLE

Greener Synthesis and Characterization, Antimicrobial and Cytotoxicity Studies of Gold Nanoparticles of Novel Shapes and Sizes

Francis J. Osonga, Idris Yazgan, Victor Kariuki, David Luther, Apryl Jimenez, Phuong Le & Omowunmi A. Sadik*

Abstract

We hereby present a novel approach for the synthesis of gold nanoparticles (AuNPs) using water soluble, naturally-derived flavonoids. Quercetin pentaphosphate (QPP), Quercetin sulfonic acid (QSA) and Apigenin triphosphate (ATRP) were utilized as reducing agents and stabilizers for the gold nanoparticle synthesis. Synthesis was achieved at room temperature using water as a solvent and it requires no capping agents. The AuNPs were characterized using Uv-Vis, X-ray diffraction (XRD), Transmission electron microscopy (TEM), Energy dispersive absorption spectroscopy (EDS), High resolution transmission electron microscopy (HR-TEM) and selected area electron diffraction (SAED). The resulting AuNPs were spherical, triangular, cubicle, hexagonal and rectangular in shape. The average particle size of 4.85 nm, 9.56 nm and 13.54 nm were obtained for the nanoparticles derived from QPP, ATRP and QSA respectively. The surface plasmon resonance peak of the AuNPs derived from QSA, ATRP and QPP was observed at 541 nm, 544 nm and 547 nm respectively. The AuNPs exhibited excellent antibacterial activities of 99.9 %, 100 % and 99.9 % growth inhibition for *Escherichia coli* ATCC® 25922™, *Staphylococcus epidermidis* ATCC® 12228™ and *Citrobacter freundii* ATCC® 8090 at 10^4 cfu inoculations. The AuNPs were observed to retain stability after 150 days compared to those reported using conventional approaches of 30 days. This work also provides insights into the mechanism of flavonoid-based nanoparticle synthesis while eliminating the use of hazardous and toxic organic solvents and adopting the use of water as a solvent.

KEYWORDS: Flavonoids, greener synthesis, gold nanoparticles, spherical, triangular, cubicle, hexagonal, rectangular, aqueous solvent and antibacterial activity

1.0 INTRODUCTION

Currently there is a demand for synthetic methods that utilize fewer amounts of materials, water, and energy; while reducing or replacing the need for organic solvents. Notable developments include Safer-by-design concepts, biologically-inert SiO_2, microwave irradiation, and the use of biomass precursors. However, chemical methods normally use reducing agents such as sodium borohydrate to reduce Au^{3+} to Au^0 and stabilizer such as polyvinylpyrrolidine is required to control particle growth thereby preventing aggregation. The integration of non-toxic and natural substances in nanotechnology is a key step towards the use of greener chemistry. Green chemistry has gained much momentum as an alternative means of carrying out studies in modern science research. The use of environmentally-friendly approaches to tackle problems and perform experiments has become an emerging trend and mindset.[1-10] Also gaining a high degree of attention is the synthesis of AuNPs in the field of nanotechnology in modern material sciences.[3-6] Gold nanoparticles, in particular, possess numerous properties such as electrical, magnetic, and thermal conductivity, chemical and biostability, catalytic activity, antibacterial activity, anti-HIV activity, antimalarial agent, and anti-arthritic activity that allow them to be used in an extensive range of applications in medicine, catalysis, electronics, photonics and biotechnology.[2, 3, 5, 11, 12]

[a.] Address here.
[b.] Address here.
[c.] Address here.
† Footnotes relating to the title and/or authors should appear here.
Electronic Supplementary Information (ESI) available: [details of any supplementary information available should be included here]. See DOI: 10.1039/x0xx00000x

Many synthetic methods of AuNPs utilize toxic chemicals that are both biologically and environmentally hazardous. The usual procedure for AuNPs synthesis is the addition of a reducing agent to a solution of chloroaurate ions (AuCl$_4$$^-$).[4] Successful synthesis of AuNPs using traditional chemical and physical techniques have been carried out and the protocol normally requires the use of strong reducing agents such as sodium borohydride or hydrazine and organic solvents .[4, 5, 14] It is worth noting that compounds such as surfactants and polymers are also used in the synthesis of gold and other metallic nanoparticles.[3] Unfortunately, these compounds are harmful to human health and toxic to the environment. Additional disadvantages that often accompany these methods include: the requirement of intricate preparation and expensive materials and equipment, high temperature conditions, and long reaction times.[1-8] Hence these concerns can be alleviated by using greener techniques for AuNPs synthesis.

Green chemistry ultimately eliminates the use of substances that are harmful to human health and the environment, replacing them with more natural materials.[5] Plant mediated biological synthesis of AuNPs is a simple and relatively rapid process that is both economically and environmentally friendly. Plants contain natural biomolecules that can be extracted and used for the reduction of metal ions. Molecules such as citric acid, ascorbic acids, flavonoids, reductases, and dehydrogenases present in the plant may act as natural reducing agents.[1-8]. Studies have shown that tea extract — a source rich in polysaccharides, vitamins, purines, xanthine alkaloids (e.g. caffeine) and phenolic compounds could be used in AuNPs synthesis.[2,3,6-8] While entire milieu of these natural extracts have been used in nanosynthesis, it is unclear what is the active component responsible for the reduction and what is the mechanism of action. Compared to chemical and physical synthesis of AuNPs, biological synthesis is a relatively easier process that yields products with superior biocompatibility and stability.[1-3, 6] Further, biological synthesis allows for good control of the size and shape of the nanoparticles.[1, 2, 4, 6-8, 15, 16] It is worth noting that non-spherical gold nanoparticles show unique electronic and optical properties which make them to be suitable candidates for applications in optical sensing, photonics, electronics and biomedical modelling. It has been reported that AuNPs synthesized by chemical or physical means aggregates under physiological conditions and this may hamper their possible in vivo applications such as drug delivery[2]and in particular the antibacterial activities of nanoparticles have been studied extensively in the recent years.[17-28] Green synthesized silver and gold nanoparticles have been used in detection of chromium (VI), copper (II), and mercury in aqueous solutions.[29-33]

In this paper we report for the first time the greener synthesis of Au nanoparticles of different shapes and sizes using water soluble, phosphorylated and sulfonated Quercetin, including QPP, QSA, and ATRP. These flavonoids served as the reducing and capping agent thereby forming stable spherical, triangular, hexagonal, cubicle and rectangular AuNPs. In this case the flavonoid derivatives are also being used as a stabilizer thereby avoiding use of organic chemicals.

2.0 MATERIALS AND METHODS

2.1 Materials

All chemicals were of analytical or reagent grade and were used without further purification. Apigenin was purchased from Indofine Chemicals Inc. (Hillsborough, NJ). Hydrogen tetrachloroaurate (HAuCl$_4$•3H$_2$O), 4-dimethyl amino pyridine, palladium 5% on activated carbon were purchased from Sigma-Aldrich, Milwaukee, WI. Methylene chloride, carbon tetrachloride (CCl$_4$), dibenzyl phosphite, N, N-diisopropylethyllamine (DIPEA) and acetonitrile, were purchased from Sigma-Aldrich (St. Louis, MO). Methanol, hexane, ethyl acetate, sodium chloride (NaCl), anhydrous sodium sulfate (Na$_2$SO$_4$) and potassium dihydrogen phosphate (KH$_2$PO$_4$) were purchased from Fisher Scientific, Pittsburg, PA. Anhydrous quercetin was purchased from MP Biomedicals, LLC, Solon, Ohio. All reagents were prepared using Nanopure water with a specific resistivity of 18 MΩ cm. All reactions involving air or moisture sensitive reagents or intermediates were performed under Ar or N$_2$ atmosphere.

2.2. Instruments

UV/Vis spectroscopy studies of gold nanoparticles were carried out on a HP 8453 UV- visible diode array spectrophotometer. Analytical TLC was performed using 0.25 mm EM Silica Gel 60 F250 plates visualized by UV irradiation (254 nm). Purification of products was carried out by flash chromatography Combiflash companion/TS Model serial 207L20329, Teledyne Isco, Inc,. ^{1}H, ^{13}C, ^{31}P NMR spectra were obtained using 600 MHz Bruker Avance. XRD was performed using Philips X'pert MPD. TEM measurements were carried out in a JEOL TEM 2100F. Dynamic light Scattering analyses were carried out on DLS- Zetasizer model ZEN 3600, Malvern Instrument Ltd. United Kingdom. FT-IR data was collected on Perkin Elmer Spectrum *65* FT-IR spectrometer (Waltham, MA). The samples were dissolved in deionized water and then dropped onto Polyethylene IR Card (International Crystal Labs.,Garfield, NJ) and left to dry in fume hood for 24 hours..

2.3. Synthesis of QPP, QSA and ATRP

The synthesis of QPP and ATRP followed the procedure described in literature[35] with slight modification in the use of equivalents in chemicals for phosphorylation. However in the case of QPP and ATRP catalytic hydrogenation at ambient temperature under pressure of hydrogen was used for debenzylation purposes.[36] The synthesis of QSA followed procedure in literature [37] but with modification. Solubility studies show that QPP and QSA have at least 84000 and 2700 fold enhancement in solubility over the unmodified QCR respectively. On the other hand ATRP showed 3660 fold solubility enhancement over the parent molecule apigenin.

2.4 Synthesis of Gold Nanoparticles

The reduction of Au^{3+} ions to Au^0 was achieved using QPP, QSA and ATRP both as reducing and stabilizing agents. In this case 4 mg of QPP, QSA and ATRP were each added to separate 50 mL vials and then 5mL of Nanopure water was added to each set up and then hydrogen tetrachoroaurate was added followed by the addition of 1mM freshly prepared Hydrogen tetrachloroaurate ($HAuCl_4 \bullet 3H_2O$). All solutions were prepared in clean, dry 50 mL vials using a 4 mg sample of the flavonoid derivative being studied, a 2 mL aliquot of aurate solution ($HAuCl_4 \bullet 3H_2O$) and 5 mL of distilled Nanopure water. During time-dependent studies, samples were allowed to rest at room temperature (25°C) under observation for significant color change. During temperature-dependent studies, samples were heated in a thermostated water bath. All spectrophotometric readings were taken using an Agilent Technologies 8453 UV-Vis Spectrophotometer. Many solutions precipitated visible quantities of nanoparticles. The AuNPs solutions were sonicated for 35 minutes in an ultrasound bath and then centrifuged at 3500 rpm for 10 minutes and the pellets formed were washed three times with 18MΩ cm resistivity Nano pure water to remove any unreacted flavonoid derivatives and $HAuCl_4 \bullet 3H_2O$.

2.5   Antibacterial studies

Antibacterial activity of AuNPs was tested using gram positive and gram negative bacteria. Utilizing Mueller Hinton Agar 2, different concentrations of silver nanoparticles (20 μg/mL to 0.2 μg/mL) were applied to *Staphylococcus epidermidis* ATCC® 12228™, *Escherichia coli* ATCC® 25922™ and *Citrobacter freundii* ATCC® 8090 as model microorganisms.

2.6 Cell cytotoxicity studies

Cytotoxicity of gold nanoparticles was tested at concentrations between 5-20 μg/mL on IEC-6 cells in DMEM medium using 0.1μg/mL Bovine insulin, 10% FBS and 1% penicillin & streptomycin mixture. Cytotoxicity was tested via non-cancerous immortalized rabbit intestinal cell line, IEC6 cells. 1 mL of 10^4 cells/mL IEC-6 cells was seeded in 24-well plate and then autoclave-sterilized gold nanoparticles were introduced to the cells in 5 μL 18.2 MΩ nano pure water. Immediately after 24 h incubation, 25 μL Presto Blue® fluorescence dye was added into each well. The cells were incubated at 37 °C under 5 % CO_2 concentration for 20 min. The results were then recorded using Biotech Synergy HT Microplate Reader. Excitation/Emission was 530nm/25 and 590nm/35, and the plates were read from bottom with sensitivity of 25 (arbitrary unit).

3.0 RESULTS AND DISCUSSION

3.1 Visualizing the formation of AuNPs

Qualitative indication of the reduction of Au^{3+} ions was demonstrated by the presence of visible nanoparticles almost immediately after the addition of the flavonoid derivative and gold solution. Further visual observations confirming the formation of AuNPs were the color change phenomena that occurred from pale yellow solution to purple color (Figure S1). The purple color was attributed to reduction of Au^{3+} of QPP darkened considerably as compared to ATRP and QSA. The appearance of purple color after reaction of $HAuCl_4.3H_2O$ with the flavonoid derivatives confirmed the formation of gold nanoparticles.[4]. The appearance of the purple color could be attributed to the excitation of surface plasmon vibrations and hence was used as spectroscopic signature to show the formation of AuNPs.

3.2 UV-Vis characterization

The UV-Vis spectrophotometer enables the instrumental confirmation of the visual observation for the reduction of Au^{3+}. This is attributed to the existence of surface plasmon band which occurs due to the collective electron oscillation around the surface mode of the particles. It has been established that gold exhibits red wine color due to the excitation of the surface plasmon resonance (SPR) in aqueous solution.[38] Uv-vis spectroscopy has been widely used to determine size and shape of nanoparticles based on the SPR peaks.[16] The UV-Vis spectroscopic data obtained from the time and temperature dependence studies allowed for further characterization of the reaction products. It was also used to ascertain the optimal conditions under which the reactions may be performed. Herein, the primary objective was achievement of the most stable reaction products under the most efficient conditions. The reduction commenced within 5 minutes and was completed in 50 minutes. Figure1 shows the reduction of Au^{3+} ions by QPP showing the SPR peak of gold at 544±3 nm.[39]

ARTICLE

Journal Name
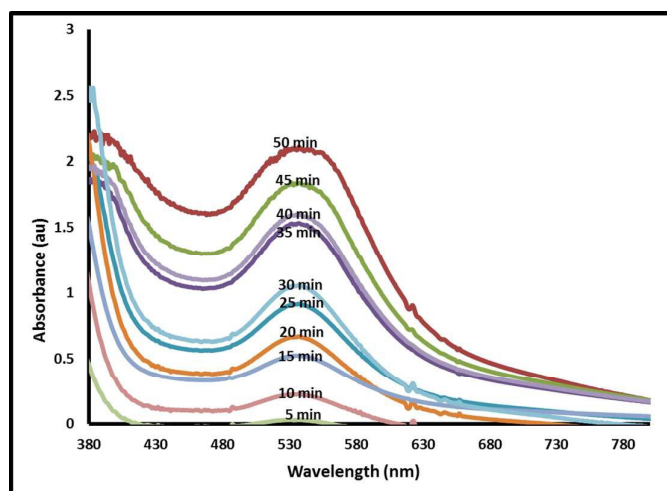
Figure1: Uv-vis absorption spectra of gold nanoparticles after reaction of 5.0×10^{-3} Au^{3+} ions with 3.5×10^{-3}M QPP recorded at different times.

It is imperative to note that within 5 minutes after the addition of Au^{3+} ions to QPP, the solution turned purple and this was accompanied with the appearance of the peak at 544 nm. The intensity of SPR peak increased from 10 minutes up to 50 minutes. It is worth noting that there was no change in the SPR peak and the formation of the purple color occurred at room temperature.

Figure 2 illustrates the Uv-visible spectra in which the SPR peaks ranged from 524nm to 544 nm thereby confirming the formation of AuNPs in solution. It has been established that the appearance of the peaks takes place as a result of the size dependent quantum mechanical phenomenon known as SPR. Furthermore SPR is predominantly influential when the De-Broglie wavelength of the valence electrons is equal to or less than the size of the particle usually < 50 nm.[40]
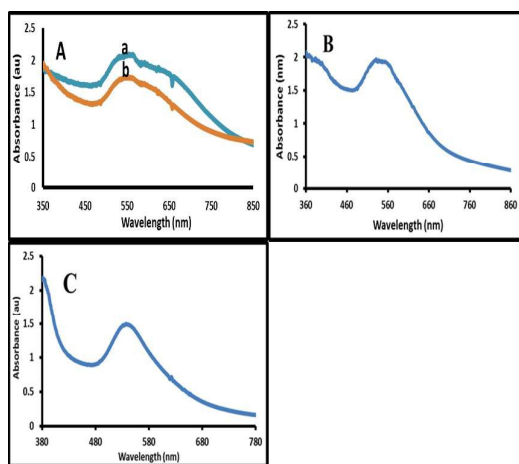
Figure 2: Uv-vis absorption spectra of gold nanoparticles after reduction with (A) (a) $3.5 \times e^{-3}$M and (b) $3.5 \times e^{-4}$ M QSA (B) $3.5 \times e^{-4}$ M QPP and (C) $3.5 \times e^{-4}$ M ATRP.

Literature sources state that SPR bands occur as a result of collective oscillations of the electron gas (6s electrons of the conduction band) of the surface of gold nanoparticles which is correlated with the electromagnetic field of the incoming light that is the excitation of the coherent oscillation of the conduction band.[41, 42] The SPR of the AuNPs consists of two components: scattering and absorption. The scattering component is known to be responsible for fluorescence enhancement and the absorption component for fluorescence quenching.[43, 44]. The average nanoparticle size was calculated as reaction progressed by applying the formula as shown in equation1.[33, 45- 46]

D = (9.8127 x 10^{-7}) λ^3- (1.7147x 10-3) λ^2 + (1.0064) λ -194.84
Equation 1

Where D (nm) is the size of any given gold nanoparticle sample, λ is the wavelength (nm) of the SPR peak of gold nanoparticles. Using this formula, we estimated the average size of gold nanoparticles derived from QPP at SPR peak of 544 nm to be approximately 3.17 nm. The SPR peak depends not only on the nanoparticle size and shape but also on some external properties of the nanoparticles environment such as dielectric constant of the medium, temperature as well as the refractive index of the solvent.[47] It can therefore be deduced that the occurrence of typical AuNPs SPR bands in the UV-vis region confirms that the AuNPs had been formed. It also indicated that the flavonoid derivatives acted as good reducing agents and as a stabilizer of AuNPs by capping the nanoparticles surfaces since no other reagents were added.

3.3 Effect of Temperature on Formation of AuNPs

All temperature studies were performed within 1 hour after initial preparation of the solution, which allows us to disregard any concerns related to time-dependent stability in the analysis of these results. As seen in Figure 3A, the potential role played by temperature in facilitating the progression of the reaction is very clear based on the UV-vis data obtained for QPP with increase in temperature was accompanied by increase in absorbance. However, the study performed under temperature-dependence with QPP shows a clear preference towards certain temperatures, with a nanoparticle peak swelling around 544 nm, and displaying most prominently around 80°C. Increase in temperature led to increase in formation of nanoparticles but at 90°C the peak decreased clearly showing that 80°C was the optimum temperature for the formation of gold nanoparticles. The color changes demonstrates the trend but at 90°C the color is totally different and the peak is not sharp implying that it led to formation of large nanoparticle.[1,7] Several reports have indicated that AuNPs were synthesized at high temperatures in order to obtain smaller sizes. For example, particle size of 4-15 nm was obtained at 105°C.[34] Although the synthesis could take place at room temperature, increase in temperature led to increase in rate of rate of collision of the reacting species due to increase in kinetic energy. The surface plasmon bands displayed blue shift from 544-538 nm with increasing absorbance. This blue shift normally indicates the formation of small spherical nanoparticles. It could be observed that at room temperature triangular gold nanoparticles were formed while the spherical nanoparticles were formed at temperatures of 80°C (Figure S2). This can be attributed to the fact that higher temperatures may trigger the nucleation process at the expense of the secondary reduction process and further condensation of a metal on the surface of nascent nanoparticle.[48]
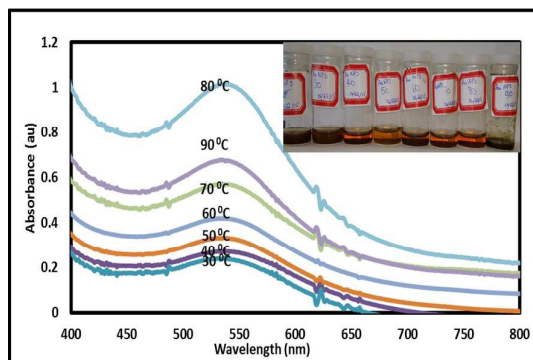
Figure 3A: The effect of temperature on the formation of AuNPs from reduction of Au^{3+} by QPP at different temperature values ranging from 30°C to 90°C. Inset is the color change at different temperatures.

The study revealed that increase in temperature led to increase in the efficiency of Au^{3+} reduction. This is due to increase in reaction rate between the Au^{3+} and the flavonoid derivative thereby leading to a faster reduction of Au^{3+} than at room temperature. The Au nanoparticles formed at higher temperatures were more crystalline in nature than those prepared at room temperature (Figure S 4A) probably due to the fact that higher temperatures led to increase in the nucleation rate. [48] It has been established that the position of the SPR peak generally depends on the shape and size of the nanoparticles with the observed symmetric SPR band with a single peak attributed to spherical shape of nanoparticles.[20] Change in temperature seems to have an effect on their size or intensity, which may suggest that temperature, makes it kinetically favorable for the reduction of Au^{3+} by flavonoids derivatives to form gold nanoparticles. The temperature dependence study for the reaction with QPP provided more promising evidence that temperature may indeed play a role in the extent of complexation.

3.4 Effect of Concentration on Formation of AuNPs

Increase in concentration increases the rate of collision of reactant particles and hence facilitates the rate of reduction of Au^{3+} to Au^{0}. In this case as depicted by Figures 3B and S3 it clearly illustrated that the increase in concentration of the reducing agent i.e. the flavonoid derivatives increased the intensity of the SPR peaks. It is therefore justified from Figure 3b that the resultant color of the nanoparticle solution depends on the concentration of the reductant.

As seen in Figure 3B, as the concentration of QPP increased the solution color became more dark purple (inset E). It has been revealed that the higher the concentration of the reducing agent, the smaller is the nanoparticle size obtained.[3, 7, 17] The result (Figure 3b) showed that increase in concentration of QPP lead to change in SPR peak from 534 to 570 nm and this red shift could be

attributed to an increase in the particle size. Figure S 3 illustrates the reaction of different concentration of ATRP with 5 .5 x10^{-5} Au^{3+} ions in which increase in concentration of ATRP led to increase in SPR band indicating increased formation of nanoparticles by the reduction of Au^{3+} to Au^{0}. Increase in concentration of ATRP led to blue shift from 550-534 nm and formation of narrow SPR bands depicting small spherical nanoparticles had been formed (Figure S3). Furthermore increase in concentration led to increase in absorbance clearly indicating the concentration of nanoparticles also increased.
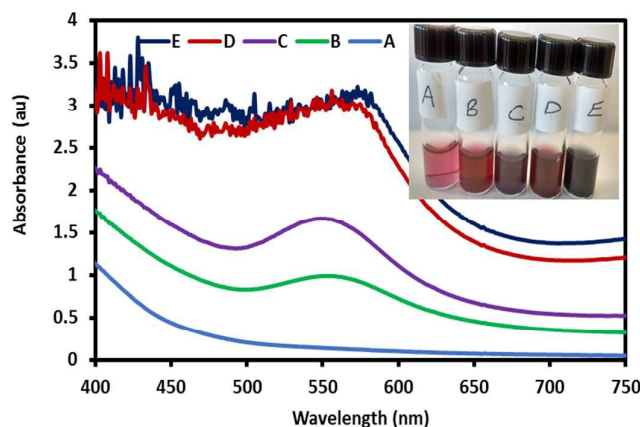

Figure 3B: Uv-Vis spectra showing dispersion of different sizes of gold nanoparticles at different molar concentrations of QPP: (A) 3.5 x 10^{-6}; (B) 3.5 x 10^{-5}; (C) 3.5 x 10^{-4}; (D) 3.5 x 10^{-3}; (E) 3.5 x 10^{-2} in the presence of 5.0 x10^{-3}M Au^{3+} ions solution. Inset: the color changed from light purple (A) to very dark purple (E) depicting the formation of AuNPs.

It is imperative to note that the wavelength shift observed in SPR bands as shown in Figure S2 is as a result of different concentration amounts of ATRP added to reduce the Au^{3+} ions. It is evidenced that the concentration of ATRP determines the size of the AuNPs as depicted by the narrow SPR bands (SPR became narrower as concentration increased from E to A with A being the most narrower). The formation of sharp bands indicated the formation of spherical AuNPs with A giving the most spherical nanoparticles. The fundamental attribute of the spherical AuNPs is its ability to act as nuclei growth centers in which the deposition of AuNPs took place.[49]

Although less concentration of flavonoid derivatives have the ability to reduce Au^{3+} to Au^{0}, they do not have the ability to act as capping agents and stabilizer as compared to the highly concentrated flavonoid derivatives (Figure 3B). Higher concentration led to narrower peaks which suggested that the smaller sizes of the AuNPs had been formed. It also indicates that when high concentration of flavonoid derivatives were used it stimulated strong interaction between the protective flavonoid derivatives and the surface of AuNPs; preventing AuNPs from sintering thus resulting in size reduction of AuNPs.[2, 48]

3.5 Stability Study of AuNPs

The synthesized AuNPs from flavonoid derivatives were found to be very stable even after 150 days as compared to AuNPs synthesized by other method which was found to be stable for 30 days.[17] The stability of AuNPs was studied for a period of 150 days and was assessed by the presence of stable SPR positions at 544 nm and the purple color (Figure 4). This is an indication that no aggregation of the nanoparticles took place. Studies have suggested that the stability of AuNPs may be as a result of potential barrier which develops due to competition between weak Van der Waals forces of attraction and electrostatic repulsion.[17]

Furthermore, the stability of AuNPs may be due to the protection by the flavonoid derivatives which act as a capping agent.
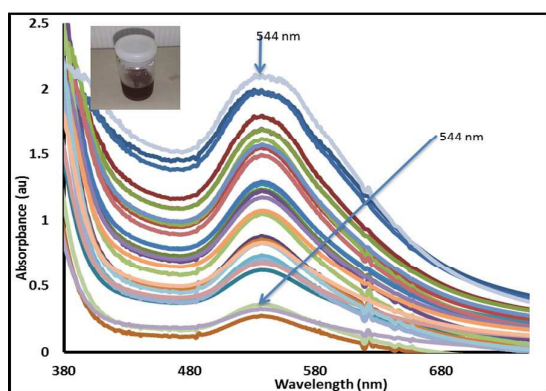

Figure 4: Uv-vis spectra showing the stability of AuNPs for a period of 150 days with no change in SPR peak position or color. Inset: The purple color of AuNPs remained unchanged

3.6. TEM Characterization

TEM images of gold nanoparticles derived from ATRP, QPP and QSA are shown in Figure 5A: a and b; c and d; e and f; respectively. TEM confirmed the formation of gold nanoparticles and gave clear morphology of AuNPs. These also indicate that the AuNPs formed were largely spherical. However, triangular, cubicles, rectangular, hexagonal nano-prism shaped were also formed. The nanoparticles were in the range of 2-20 nm, 2-30 nm and 3- 45 nm for ATRP, QPP and QSA respectively. It can be clearly seen that a mixture of nano-prism; rectangular, cubicle, spherical, hexagonal and triangular structures were obtained (Figure 5A). Nano-triangles were formed (Figure 5A) due to rapid reduction, assembly and sintering of spherical nanoparticles at room temperature, rearrangement and aggregation of smaller size AuNPs.[24] The formation of triangular AuNPs acted as a nuclei for further growth into anisotropic triangular structures.[24] It is worth noting that non-spherical gold nanoparticles show unique electronic and optical properties which make them to be suitable candidates for applications optical sensing, photonics, electronics and biomedical modelling. [50] Gold nanoprisms and icosahedral

have been synthesized by using seed mediated, iodide ion and cetyltrimethylammonium bromide CTABr protocol as capping agent to control nanoparticle size. The seeds were obtained by reduction of $HAuCl_4$ using $NaBH_4$ in the presence of sodium citrate which acted as a capping agent.[51,52] The TEM images in Figures 5A and 5B show that nanoprisms were synthesized by reduction of Au^{3+} using flavonoid derivatives acting as capping agent and stabilizer with no extraneous reagents or the use of ng organic solvents.

Figure 6 (a-c) shows the HRTEM images of AuNPs derived from ATRP, QPP and QSA respectively. HRTEM was undertaken in order to understand the sizes and topology of AuNPs. HRTEM images shown in Figure 5 (a-c) exhibited good crystalline structure depicting that particles were internally twinned. It has been established that face centered cubic (fcc) structured crystalline metallic nanoparticles normally nucleate and thereby grow into remarkable twinned nanoparticles with their surfaces bounded by the lowest energy facets (111).[53] The fringes observed in HRTEM images showed that the flavonoid derivatives acted as a good reducing agent for Au^{3+} in water. Single crystalline particles were formed oriented in same way.
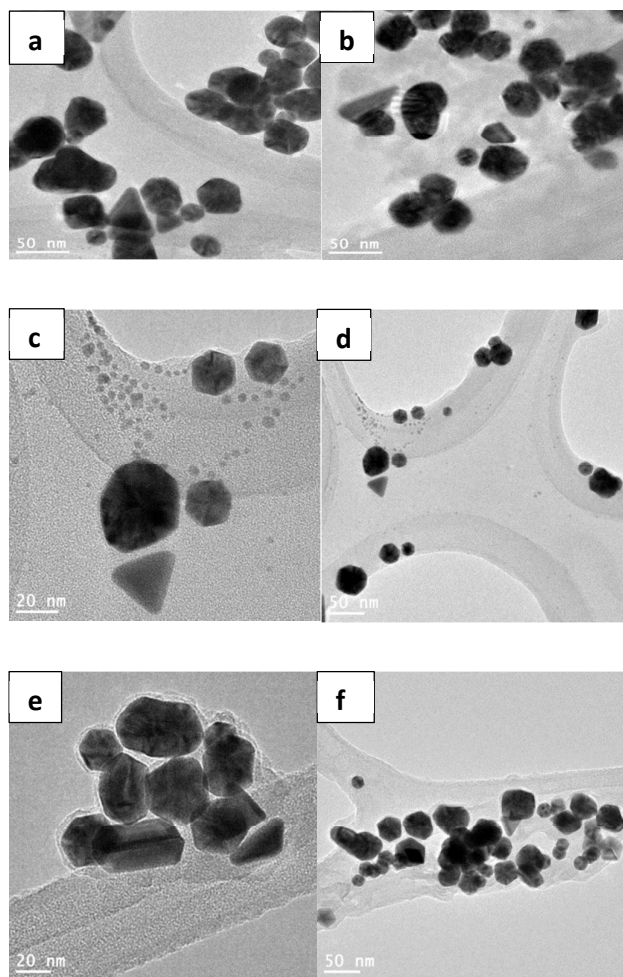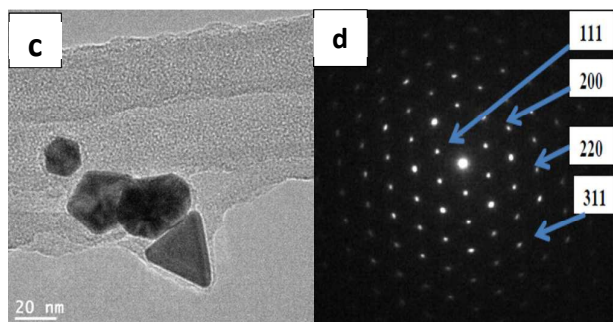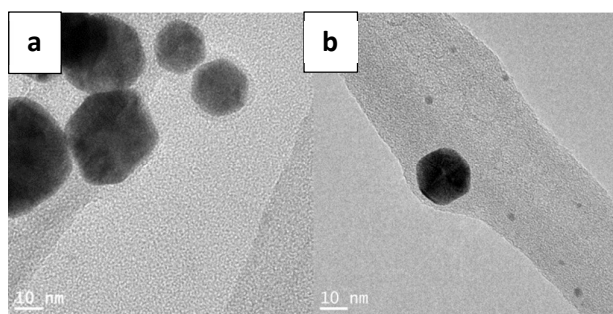

Figure 5A: TEM micrographs showing AuNPs derived from ATRP (a and b); QPP (c and d) and QSA (e and f).

Figure 5B: HRTEM images of AuNPs at different magnifications of a, b and c obtained from ATRP, QPP and QSA respectively; (d) SAED crystallinity of Ag NPs derived from QSA.

The selected area electron diffraction (SAED) pattern of AuNPs corresponds to (111), (200), (220) and (311) confirming that the nanoparticles were crystalline in nature [Figure 5B (d)].

DLS was used to determine the hydrodynamic diameter of AuNPs present in the aqueous solution (Figure 6). The average diameter size of AuNPs derived from ATRP (Figure 6a was determined to be 12.64 nm±2.854 with Z-average of 89.04 nm. DLS measurements clearly depicted the AuNPs derived from QPP (Figure 6b) were of average size of 3.063±0.7509. However the Z-average for AuNPs determined was estimated to be 51.04 nm. As shown in Figure 6c, the average size of AuNPs derived from QSA was found to be 86.12 nm±25.75 Z, whereas the average of AuNPs derived from QPP was determined to be 86.50 nm.
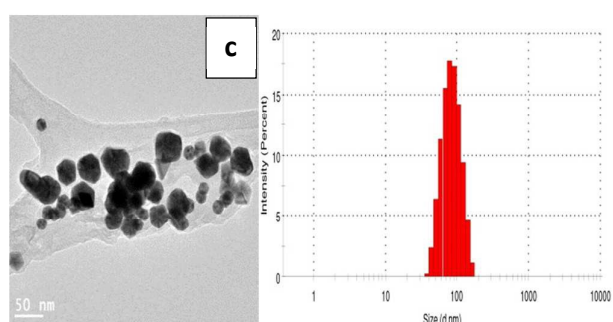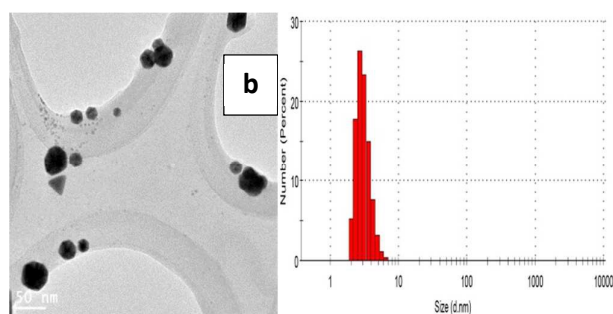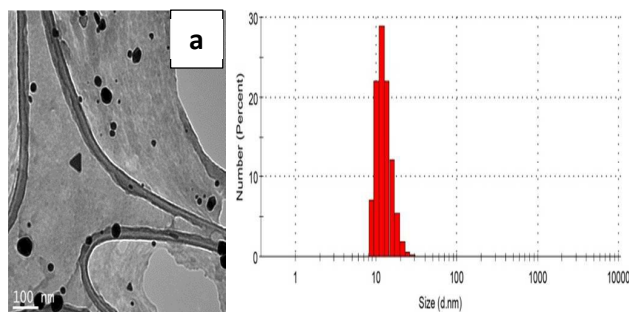
Figure 6: TEM image of AuNPs derived from (a) ATRP, (b) QPP and (c) QSA including their respective DLS particle size distribution.

Figure 7a and Figure S4A showed the EDS analysis of AuNP sample obtained using ATRP and QPP respectively. The result confirmed the formation of gold atoms at 2.00 keV and 10.00 keV with higher amount of gold at 2.00 keV. This phenomenon takes place because of gold nanocrystallite absorption due to SPR of metallic gold nanocrystals.[17]
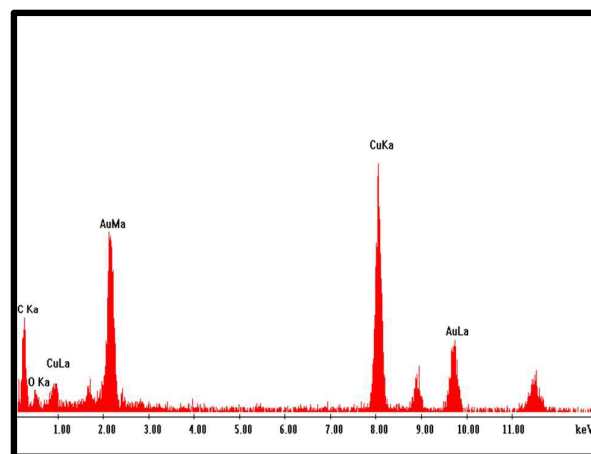
Figure 7a: EDX spectrum confirming formation of AuNPs derived from ATRP.

The result of EDS analysis clearly showed the presence of elemental gold and hence is in agreement with the XRD results. It

is worth noting that since gold nanoparticles were drop coated on carbon coated copper grid, the peaks for Cu and C are basically from the grid used.

3.7.1 X-ray Diffraction Characterization

XRD is a very important tool used for the determination of the crystal structure of nanoparticles and also applied to calculate the crystalline nanoparticle size. Similar to the HRTEM data, XRD analysis confirmed the formation of AuNPs. Figure 7b shows the XRD pattern of AuNPs obtained from QPP depicting 4 characteristic diffraction peaks at 2θ = 38.08°, 44.26°, 64.45°, 77.40° which can be indexed to (111), (200), (220) and (311) (Joint Committee on Powder Diffraction Standard, JCPDS No. 04-0784) Bragg reflections of fcc structure of gold respectively. These depict that pure crystalline gold has been synthesized. The XRD results (Figure 7b) also demonstrate that the gold nanoparticles obtained from naturally-derived flavonoids are crystalline in nature. Figure S4B shows the XRD pattern of AuNPs derived from ATRP and QSA confirming the crystallinity of the nanoparticles.
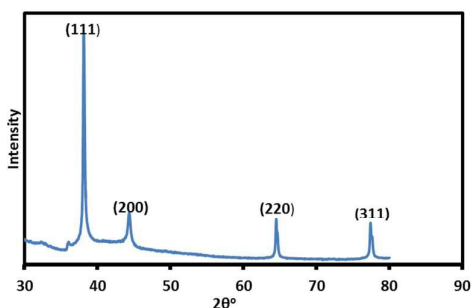

Figure 7b: XRD pattern of gold nanoparticles derived from QPP

The intensity of the peaks further shows that the synthesized AuNPs are of high degree of crystallinity and hence the flavonoid derivatives are able to reduce Au^{3+} and stabilize the Au nanoparticles formed. It has been established that the peaks at 2θ=38.08°, 44.26°, 64.45° and77.40° generally correspond to gold peaks (Joint Committee on Powder Diffraction Standard, JCPDS No. 04-0784).[2, 5, 6, 8, 17.] The average crystalline size of the AuNPs was determined from the peak broadening using Debye-Scherrer formula [6,29]; d = Kλ/β Cosθ, Where; d = the crystalline particle size of nanoparticles; K = the Scherrer constant (values always range from 0.9-1 usually taken for a cubic system); λ = the wavelength of X-ray radiation (1.5406Å= 0.15406 nm) which is used in XRD; β = is the full width at half the maximum intensity of the diffraction peak of (111) Brag reflection generally in radians and θ = the Bragg angle.

The formula was used to calculate the average particle size which was found to be 4.85 nm, 9.56 nm and 13.54 nm for the AuNPs derived from QPP, ATRP and QSA respectively. This is in agreement with TEM results (Figure S5-S7). Based on the XRD data (Figure 7b), the peak with the major peak intensity is assigned 111

and using the d spacing of 2.34Å with the crystal maker software the formulation for modelling nanocube was adapted based on crystal maker software. The length of the nanocube was obtained as 4.053 Å and the expansion factor of 95.6/4.053 = 23.6 which was used to expand the unit cell and draw the AuNPs (Figure 7c and S8).
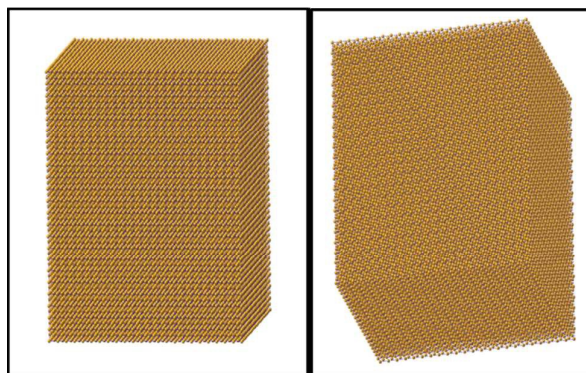

Figure 7c: Face centered cubic model of the AuNPs showing the packing of the gold atoms in the nanocubes as obtained from crystal maker software.

3.7.2 Fourier Transform Infrared Spectroscopy (FTIR)

FTIR measurements were conducted in order to identify the functional groups that are responsible for the excellent reduction, capping and stabilization of AuNPs. Figure 8A shows the the FTIR spectra of ATRP (a) and ATRP-AuNPs (b) Aromatic C-H stretching for ATRP and ATRP-AuNPs all occurred at 1464 cm^{-1}. The band at 1604 cm^{-1} is assigned to C=O stretch of the ATRP molecule. The C=O is present in flavonoid molecules at 4-oxo position. There is a change in this band from 1604 cm^{-1} in Figure 8A (a) to 1650cm^{-1} in Figure 8A (b) and this shift suggests that the keto group in ATRP is involved in the reduction of AuNPs. The remaining bands remained the same.

The FTIR spectra of QPP and QPP-AuNPs are shown in Figure 8B (a) and (b) respectively. The C=O stretch is seen at 1660 cm^{-1} in Figure 8B (a). This C=O band is in agreement with the band observed for the parent molecule Quercetin.[54] However this band shifts to 1694 cm^{-1} as seen in Figure 8B (b) which confirms that binding of AuNPs occurs between the 4-oxo group and the 5- phosphate group as presented in Scheme 2. The aromatic C-H in QPP and QPP-AuNPs remained the same at 1474 cm^{-1} as shown in Figure 8B. A new band at 2416 cm^{-1} could be assigned to C-H stretching vibrations of –CH$_2$ functional group and this stretch could be caused by binding of AuNPs. The C-OH stretching band at 1030cm^{-1} Figure 8B (a) reduced significantly in 8B (b).

Figure 8C shows the spectra of QSA (a) and QSA –AuNPs (b). The O-H broad band at 3502-3050 cm^{-1} [Figure 8C (a)] may be assigned to the presence of water. However, this band disappeared in QSA-AuNPs [Figure 8B (b)] suggesting that there could have been an interaction between the Au and QSA.The aromatic C=O band at

1698 cm^{-1} in QSA Figure 8C (a) did not occur in QSA-AuNPs and this could be due to possible interaction of C=O with AuNPs. New bands occurred at 2066cm^{-1} and 2406cm^{-1} respectively; implying that binding of AuNPs to QSA could have caused the stretch which is associated with –CH$_2$ stretch. It is worth noting that aromatic C-H shifted slightly from 1474 cm^{-1} (QSA) to 1472 cm^{-1} QSA-AuNPs.
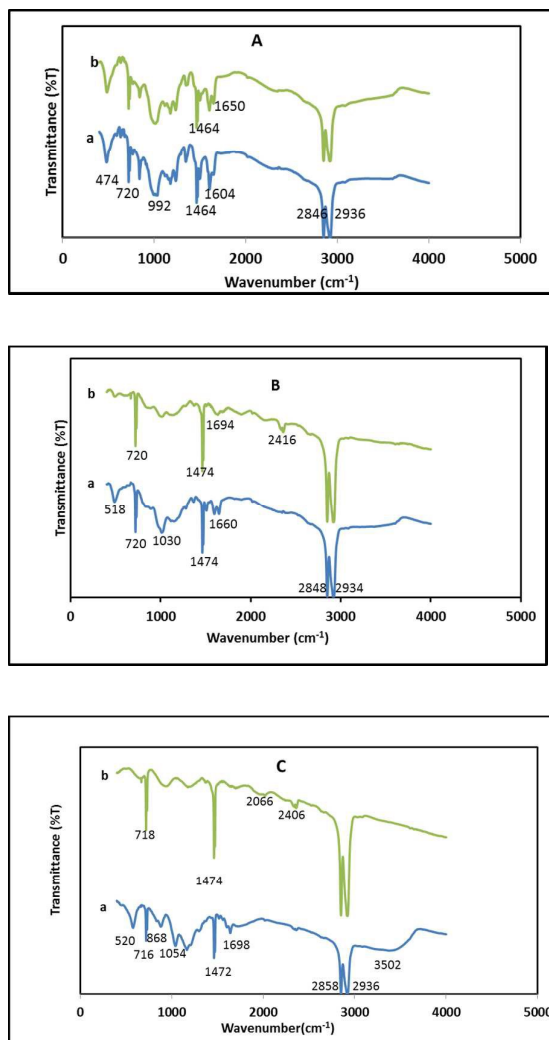

Figure 8: FTIR spectrum A ATPRP (a) ATRP-Au (b); B QPP (a) QPP-Au (b); C QSA (a) and QSA –Au (b)

**3.8 Possible Reaction Mechanism for the Formation of AuNPs**

Flavonoids are able to form complexes with metals ions. Studies have shown that complexation usually occurs at the 3' and 4' carbon position of the flavonoid followed by 3 and 4-oxo groups as the first sites for complexation.[54, 55] However complexation between the 4-oxo and 5-carbon position is not feasible due to the

fact that the proton in the –OH group of the phosphate group at this position is less acidic and is not easily protonated. Furthermore the steric hindrance due to complexation[56] between 4-oxo and 3- phosphate group Scheme 1 shows the complexation between QPP and Au^{3+} ions. The flavonoid derivatives possess good chelating properties. The phosphate group plays a significant role in this complexation process because it contains the oxygen containing functional groups like hydroxyl groups. The presence of oxo groups at carbon atom number 4 also allows complexation between the hydroxyl group of the 3- phosphate group and 4-oxo group.
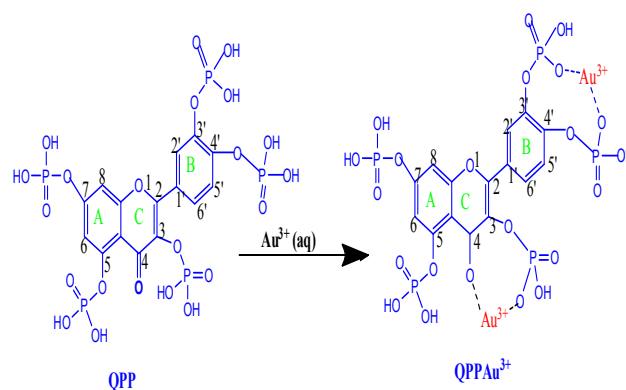
**Scheme1:** Complexation of Au^{3+} with QPP derivative at position 3', 4' and position 3 and 4-oxo sites.

The flavonoid derivative complex will tend to be unstable and hence reduction implies that QPP, QSA and ATRP act as reducing reagent and capping agent. The ionized groups on QPP are able to stabilize the gold nanoparticle as shown in Scheme 2.
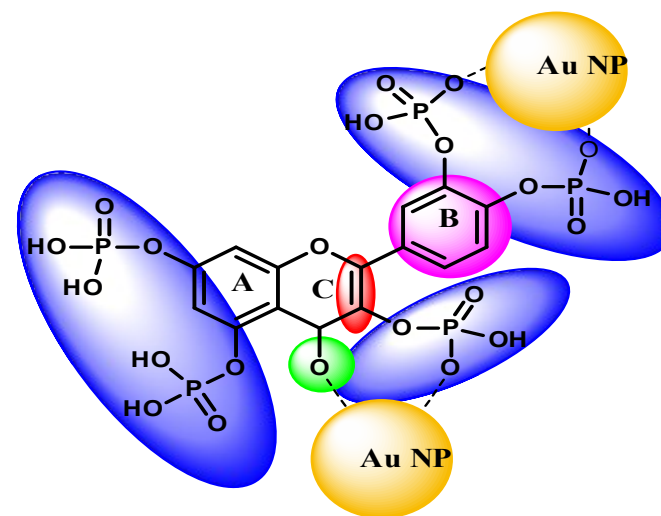
Scheme 2: Stabilization of AuNPs by QPP

The chemistry of the reduction of Au^{3+} by the flavonoid derivatives is given by Equations 1 and 2.

$$3QH_2 \longrightarrow 3Q + 6H^+ + 6e^- \qquad (1)$$

$$2Au^{3+} (aq) + 6e- \longrightarrow 2Au (s) \qquad (2)$$
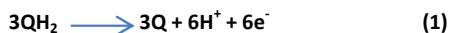
Where QH_2 represent QPP, QSA and ATRP and Q represents the product formed after complexation (quinone) in each case.

3.9.1 Antibacterial Activities of AuNPs

Antibacterial activity of the synthesized AuNPs was tested using gram positive and gram negative bacteria. Utilizing Mueller Hinton Agar 2, different concentrations of gold nanoparticles (10 µg/mL to 0.2 µg/mL) were applied to *Staphylococcus epidermidis* ATCC® 12228™, Escherichia *coli* ATCC® 25922™ and *Citrobacter freundii* ATCC® 8090 as model microorganisms.
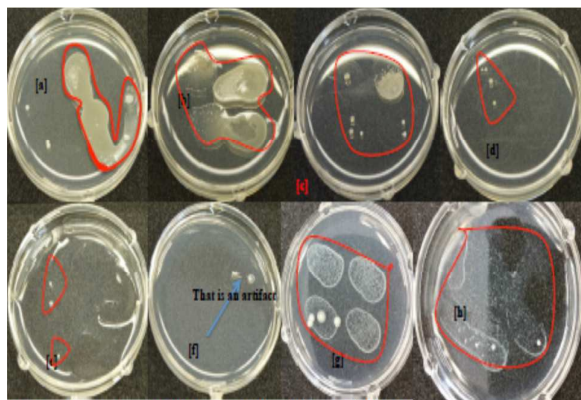

Figure 8a: *E. coli* activities of AuNPs; (a) Control (b) 200 ng/mL (c) 800 ng/mL (d) 2 µg/mL (e) 3 µg/mL and (f) 5 µg/mL. Control plate was incubated with one drop of 10^4 and 10^5 cfu *E.coli* in 20 µL. (g) and (h) 72 h incubation of 2 and 3 µg/mL AuNPs treated plates, respectively.

AuNPs treated plates were incubated with two drops of 10^4 and 10^5 cfu *E.coli* in 40 µL. As observed in Figure 8a 200 ng/mL AuNPs did not provide any significant bacterial inhibition. 800 ng/mL AuNPs treated plate showed strong inhibitory effect on *E.coli* growth, especially at 10^4 cfu E.coli inoculation with over 99.9% *E.coli* growth inhibited. 2 and 3 µg/mL AuNPs treated plates did not show any meaningful E.coli growth for 24 h incubation, whereas 72 h incubation revealed that E.coli survived from AuNPs toxicity and showed some level of growth. Moreover, the colonies were discernible but extremely tiny showing total inhibition at over 99.99%. In the case of 5 µg/mL AuNPs treated plate, no meaningful growth was observed at 72 h incubation.

Citrobacter freundii was introduced into the plates as two drops of 10^4 and 10^5 cfu in 20 µL carriers (Figure S9). 200 ng/mL AuNPs treatments did not provide any significant toxicity on *C. freundii* while AuNPs started showing their toxicity at 2 µg/mL concentration. However, 2 µg/mL AuNPs treatment inhibited *C. freundii* growth at over 99.9% using 10^4 cfu inoculations while the inhibitory effect was less than 50 % in the case of 10^5 cfu inoculations. The inhibition effect of AuNPs for 10^5 cfu inoculation became significant at 3 µg/mL concentrations with colonies becoming discernible (Figure S9). Moreover, at 5 µg/mL treatments, no colony formation was observed at 72 hours incubation.

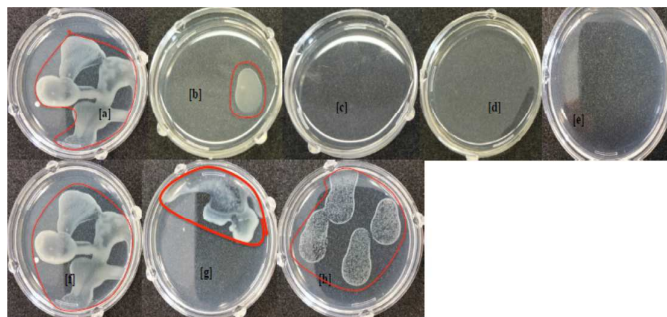Figure 8b: *S. epidermidis* activities of AuNPs. (a) Control, (b) 800 ng/mL AuNPs,(c) 2 µg/mL,(d) 3 µg/mL, and (e) 5 µg/mL AuNPs treated plates.

S. epidermidis was introduced into the plates as two drops of 10^4 and 10^5 cfu in 20 µL carrier. Even though at 24 h incubation, AuNPs showed some inhibitory effect on *S. epidermidis* growth in comparison to control, at 48 h incubation, results showed that 800 ng/mL AuNPs treatment did not possess any significant toxicity on *S. epidermidis* growth (Figure 8b). Similarly, at 2 µg/mL AuNPs treatment, no colony formation was observed for 24 h whereas the 72 h incubation showed abundant colony formation especially at 10^5 cfu inoculation. Moreover, 3 µg/mL AuNPs treatment inhibited *S. epidermidis* growth at over 99.9% even at 72 h incubation while at 24 h incubation, no colony formation was observed. Similar observation was recorded at 5 µg/mL AuNPs treatment at 72 h incubation.

AuNPs were tested for their potential bacteriostatic and bacteriocidal effects and from the results it could be deduced that AuNPs possessed bacteriostatic and bacteriocidal effects. However, this effect was directly dependent on both AuNPs concentration and inoculum concentration as detailed in Supplementary Figure S10. The age of the bacteria used in the toxicity study were kept in the log phase. It was observed that 5 µg/mL AuNPs was enough to inhibit the growth of 10^5 cfu inoculum. Even though at concentrations below 5 µg/mL; AuNPs showed some bactericidal effect, their effect on bacteria was more of bacteriostatic action. Consequently, 5 µg/mL AuNPs can

be accepted as a strong bactericidal agent to eliminate the tested bacteria up to 10^5 cfu inoculum.

The concentration can be increased 10^6 and 10^7 cfu inoculum in the case of 8 µg/mL. Altering the addition of AuNPs to the agar did not provide significant difference. Adding AuNPs to the agar before the autoclave process slightly increased anti-bacterial activity of the nanoparticles. Although the mechanism of nanoparticles against bacteria is not very well understood, it is generally accepted that the antibacterial activity may be due to electrostatic attraction between negatively charged cell membrane of microorganism and positively charged nanoparticles.[17] Gold nanoparticles possess good chemical stability, increased surface area and small size which enhances faster interaction with microorganisms.[21,57] Furthermore, it has been established that the particles may interact with the outer membrane and may cause degradation with structural changes leading to death.[58]

3.9.2 Cytotoxicity Studies

Figure 9 depicts that IEC-6 cells are tolerant to AuNPs. 5 µg/mL AuNPs were the highest concentrations for antimicrobial evaluations of the nanoparticles to eliminate 10^5 cfu inoculum. In this study, sets of experiments were carried out to evaluate the cytotoxicity of gold nanoparticles. Quantitative evaluations of AuNPs toxicity on IEC-6 cells were performed in the cases of 10^4 cells/mL and 3×10^3 and 10^5 cells/mL inoculum concentrations, respectively. 5 µg/mL was selected as the lowest AuNPs concentration since it was the highest AuNPs concentration to inhibit 10^5 cfu/mL bacterial growths as discussed under Section 3.9.
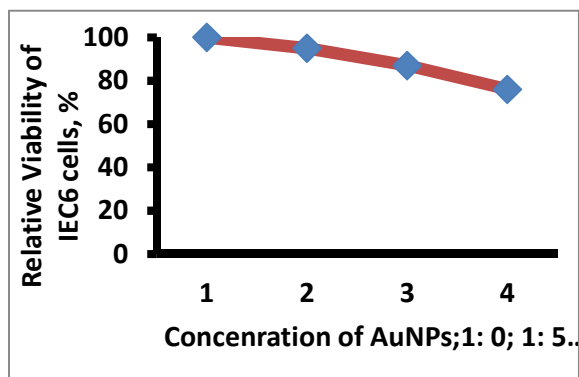

Figure 9: Percentage of viability of AuNPs on IEC6 cells.

Quantitative evaluation of the toxicity showed that, the AuNPs possessed less than 10% toxicity at 5 µg/mL AuNPs concentration (Figure 9). These results reveal that the synthesized AuNPs possessed modest cytotoxicity.

4.0 Conclusion

This study had successfully demonstrated that stable, rectangular, cubic, triangular, hexagonal, spherical gold nanoparticles have been prepared using flavonoids. The very small size obtained ranged from 2- 45 nm using water soluble naturally derived flavonoid derivatives. These reagents acted as reducing and capping agents. The UV-visible spectra confirmed the SPR position of the synthesized AuNPs. The crystalline nature of AuNPs was confirmed by XRD analysis. The synthesized AuNPs exhibit good antibacterial activities against *E .coli*, *S. epidermidis* and *C. freundii* with over 99 % inhibition.

Appendix A. Supporting data

Additional information showing the uv-vis spectra illustrating the effect of temperature on the shapes of AuNPs; the effect of formation of gold nanoparticles from reaction with different concentration of ATRP; as well as histograms showing the average particle size of AgNPs derived from QPP, ATRP and QSA. Additional data on the activity of AuNPs using Citrobacter freundii is provided. These material are available free of charge via Internet at http://dx.doi.org/…………..

REFERENCES

1. Pandey,S.; Oza, G.; Mewada, A.; Sharon, M. Green Synthesis of Highly Stable Gold Nanoparticles Using *Momordica charantia* as Nano Fabricator, *Archives of Applied Science Research*, **2012**,Vol. 4, No. 2, pp.1135-1141.
2. Boruah, S.K.; Boruah, P.K.; Sarma, P.; Medhi, C.; Medhi, O.K. Green Synthesis of Gold Nanoparticles Using *Camellia Sinensis* and Kinetics of the Reaction," *Advanced Materials Letters*, **2012**, 3(6), 481-486.
3. Sharma, R. K.; Gulati, S.; Mehta, S. Preparation of Gold Nanoparticles Using Tea: A Green Chemistry Experiment, *Journal of Chemical Education*, **2012**, 89, 1316-1318.
4. Elia, P.; Zach, R.; Hazan, S.; Kolusheva, S.; Porat, Z.; Yehuda. Green Synthesis of Gold Nanoparticles Using Plant Extracts as Reducing Agents, *International Journal of Nanomedicine*, **2014**, 9,4007-4021.
5. Parida, U.K.; Bindhani, B.K.; Nayak, P. Green Synthesis and Characterization of Gold Nanoparticles Using Onion (*Allium cepa*) Extract. *World Journal of Nano Science and Engineering*, **2011**, 1, 93-98.
6. Kamal, S. S.; Vimala, J.; Sahoo, P. K.; Ghosal, P.; Ram, S.; Durai, L., A Green Chemical Approach for Synthesis of Shape Anisotropic Gold Nanoparticles, *International Nano Letters*, **2014**, 4(109), 1-7.
7. Begum, N.A.; Mondal, S.;Basu, S.; Laskar, R.A.; Mandal, B. Biogenic synthesis of Au and Ag nanoparticles using aqueous solutions of Black Tea leaf extracts, Colloids and Surfaces B: Biointerfaces, **2009**, 71, 113-118.

8. Nadagouda, M.N.; Iyana, N.; Lalley, J.; Han, C.; Dionysios, D. D.; Varma, S.R. Synthesis of Silver and Gold Nanoparticles using Antioxidants from Blackberry, Blueberry, pomegranate, and Tumeric extracts, ACS sustainable. Chem.Eng. **2014**, 2, 1717-1723.

9. Shankar, S.S.; Ahmad, A.; Pasricha, R.; Sastry, M. Bioreduction of Chloroaurate Ions by Geranium Leaves and its Endophytic Fungus Yields Gold Nanoparticles of Different Shapes, *Journal of Materials Chemistry*, **2003**, 13(7), 1822-1826.

10. Fierascu, R.C.; Ion, R.M.; I. Dumitriu, I., Noble Metals Nanoparticles Synthesis in Plant Extracts, *Optoelectron Advanced Materials Rapid Communications*, **2010**, 4(9), 1297-1300.

11. Salata, O.V. Applications of nanoparticles in Biology and Medicine, Journal of Nanobiotechnology, **2004**, 2 (1), 3

12. Govindraju, K.; Kiruthiga, V.; Singaravelu, G. Evaluation of Biosynthesized Silver Nanoparticles against Fungal Pathogens of Mulberry Morus Indica, Journal of Biopesticides, **2008**, 1, 101-104.

13. Geddes, C. D.; Parfenov, A.; Gryczynski,I., Lakowicz, J. R. Luminescent Blinking of Gold Nanoparticles, *Chemical Physics Letters*, **2003**, 380, 269-272.

14. Ghosh, P.; Han, G.; De, M.; Kim, C. K.; V. M. Rotello, V.M.; Gold Nanoparticles in Delivery Applications, *Advanced Drug Delivery Reviews*, **2004**, 60 (11),1307-1315.

15. Kalishwaralal, K.; Barath Manikath, S.; Pandian, S.R.K.; Deepak, Venkataraman.; Gurunathan, S, Silver nanoparticles impede the biofilm formation by Pseudomonas aeruginosa and Staphylococcus epidermidis. Colloids and Surfaces B: Biointerfaces, **2010**, 79: 340-344.

16. Kumar, K.S; Kumar, G.; Prokhorov, E.; Luna-Bárcenas, G.; Buitron, G.; Khanna, V.G.; Sanchez, I.C. Exploitation of anaerobic enriched bacteria (AEMB) for the silver and gold nanoparticles synthesis, Colloids and Surfaces A: Physicochem. Eng. Aspects, **2014**, 462, 264-270.

17. Bindhu, M.R.; Umadevi, M. Antibacterial activities of green synthesized gold nanoparticles. Materials Letters, **2014**, 120, 122-125.

18. Ahmed, K.B. A.; Subramanian, S.;Sivasubramanian, A.; Veerappan,G. Preparation of gold nanoparticles using *Salicornia brachiata* plant extract and evaluation of catalytic and antibacterial activity, Spectrochimica Acta Part A: Molecular and Biomolecular Spectroscopy, **2014**, 130, 54-58.

19. Anand, K.K.H.; Mandal, B.K. Activity study of biogenic spherical silver nanoparticles towards microbes and oxidants, Spectrochimica Acta Part A: Molecular and Biomolecular Spectroscopy, **2015**, 135, 639-645.

20. Bindhu, M. R.; Rekha, P. V.; Umamaheswari, T.; Umadevi, M. Antibacterial activities of *Hibiscus cannabinus* stem-assisted silver and gold nanoparticles, Materials Letters, 2014, 131, 194-197.

21. Sreekanth, T.V.M.; Nagajyothi, P.C.; Supraja, N.; Prasad, T.N.V.K.V. Evaluation of the antimicrobial activity and cytotoxicity of phytogenic gold nanoparticles, Appl. Nanoscience, **2015**, 5,595-602.

22. Bindhu, M.R.; Umadevu,M. Antibacterial and catalytic activities of green synthesized silver nanoparticles, Spectrochimica Acta Part A: Molecular and Biomolecular Spectroscopy, **2015**, 135, 373-378.

23. Singh, K.; Pangal, M.; Kadyan, S.; Chaudhary, U.; Yadav, J.P., Antibacterial Activity of Synthesized Silver Nanoparticles from *Tinospora Cordifolia* against Multi Drug resistant Strains of *Pseudomonas aeruginosa* Isolated from Burn Patients, J. Nanmed Nanotechnol, **2014**, 5:2.

24. Bindhu, M. .R.; Umadevi, M. Silver and gold nanoparticles for sensor and antibacterial applications, Spectrochimica Acta Part A: Molecular and Biomolecular Spectroscopy, **2014**, 128, 37-45.

25. Rathi Sre, P.R.; Reka, M.; Poovazhagi, R.; Kumar, A.;Murugesan, K. Antibacterial and cytotoxic effect of biologically synthesized silver nanoparticles using aqueous root extract of *Erythrina indica lam*, Spectrochimica Acta Part A: Molecular and Biomolecular Spectroscopy, **2015**, 135, 1137-1144.

26. Lima,E.; Guerra,R.; Lara, V.; Guzmán,A. Gold nanoparticles as efficient antimicrobial agents for *Escherichia coli* and *Salmonella typhi*, Chemistry Central Journal, **2013**, 7:11.

27. Abalaka, M.E.; Daniyan, S.Y.; Adeyemo, S.O.; Damisa, D., The Antibacterial Efficacy of Gold Nanoparticles Derived from Gomphrena celosioides and Prunus amygdalus (Almond) Leaves on Selected Bacterial Pathogens, International Journal of Biological, Food, Veterinary and Agricultural Engineering, **2014**, 8(4).

28. Guzman, M.; Dille, J.; Godet, S., Synthesis and antibacterial activity of silver nanoparticles against gram-positive and gram- negative bacteria, Nanomedicine: NBM **2012**, 8, 37-45.

29. Balavigneswaran, C. K.; Kumar, T. S. J.; Packiaraj, M.; Prakash, S. Rapid detection of Cr(VI) by AgNPs probe produced by Anacardium accidentale fresh leaf extracts, Appl. Nanosci. **2014**, 4, 367-378.

30. Zhang, Z.; Li, W.; Zhao, Q.; Cheng, M.; Xu, Li.; Fang, X. Highly selective visual detection of copper (II) using water-soluble azide- functionalized gold nanoparticles and silver enhancement, Biosensors and Bioelectronics, **2014**, 59, 40-44.

31. Ravindran, A.; Elavarasi,M.; Prathna, T.C.; Raichar, A. M.; Chandrasekaran, N.; Mukherjee, A. Selective colorimetric detection of nanomolar Cr (VI) in aqueous solutions using unmodified silver nanoparticles, Sensors and Actuators B, **2012**, 166-167: 365-371.

32. Ahmed, M.A.; Hasan, N.; Shaikh, M. Silver Nanoparticles: Green Synthesis, Characterization, and Their Usage in Determination of Mercury Contamination in Seafoods, Hindawi Publishing Corporation, ISRN Nanotechnology, http://dx.doi.org/10.1155/2014/148184.

33. Mehta, V. N.; Kumar, M.A.; Kailasa, S. K. Colorimetric Detection of Copper in water Samples Using Dopamine Dithiocarbamate-Functionalized Au Nanoparticles, Industrial& Engineering Chemistry Research, **2013**, 52, 4414-4420.

34. Fleming, D.A and Williams, M.A. Size-Controlled Synthesis of Gold Nanoparticles via High-Temperature Reduction, Langmuir, **2004**, 20, 3021-3023.

35. Okello, V.A.; Zhou, A.; Chong, J.; Knipfing, M.T.; Doetschman, D & Sadik, O.A. Reduction of Hexavalent Chromium using Naturally-derived Flavonoids, Environmental Science & Technology, **2012**, 46(19), 10743–10751.

36. Silverberg L. J.; Dillon J. L.; Vemishetti P. Simple, Rapid and Efficient protocol for the selective phosphorylation of phenols with Dibenzyl Phosphite. *Tetrahedron Lett*. **1996**; 37(6): 771 – 774.

37. Kopacz, M. Quercetin and morin sulfonates as analytical reagents. J. Anal. Chem. **2003**, 58 (3), 225-229.

38. Mulvaney, P. Surface plasmon spectroscopy of nanosized metal particles, Langmuir, **1996**, 12:788.

39. Noginov,M.A.;Zhu,G.;Bohoura,M.;Adegoke,J.;Small,C.;Ritzo,B.A.;Drachev, V.P.; Shalev, V.M., The effect of gain and absorption on surface plasmons in metal nanoparticles, Appl Phys B. 2007, 86:455.

40. Henglein, A. A physicochemical property of small metal particles in solution: "microelectrode" reactions, chemisorption, composite metal particles, and the atom- to- metal transition. J. Phys. Chem. **1993**, 97, 5457-5471.

41. Daniel, M.C.; Astruc, D.A. Chemical Reviews,**2004**,104(1): 293-346.

42. Huang, X.; Jain, P.K.; El-Sayeed, I. H.; El-Sayeed, M.A.; Nanomedicine, **2007**, 2(5),681-693.

43. Nasir, S. M.; Nur, H. Journal of Fundamental Sciences, **2008**,4,245-252.

44. Drozdwicz-Tomsia,K.; Goldys, E.M. MQ BioFocus Research Center, Macquarie University, NSW, Australia. "Gold and Silver Nanowire for Fluorescence Enhancement", Nanowires-Fundamental Research, Page 309-332.

45. Yu, W. W.; Qu, L. H.; Guo, W. Z.; Peng, X.G. (2003) Experimental determination of the extinction coefficient of CdTe, CdSe, and CdS nanocrystals. Chem Mater, **2003**, 15: 2854

46. Wu, H.; Liang, J.; Han, H. A novel method for the determination of Pb2+ based on the quenching of the fluorescence of CdTe quantum dots.Microchim. Acta. **2008**,161, 81-86.

47. Li, C.Z.; Male, K.B.; Hrapovic, S.; Luong, J.H.T. Chem.comm., **2005**, 3924-3926.

48. Makarov, V.V.; Love, A.J.; Sinitsyna, O. V.; Makarova, S. S.; Yaminsky, I. V.; Taliansky, M.E.; Kalinina, N.O. Reviews "Green" Nanotechnologies: Synthesis of Metal Nanoparticles Using Plants. Acta Naturae, **2014**, 6, 1(20), 36-44.

49. Kasthuri, J.; Veerapandian, S.; Rajendiran, N. Colloids and Surfaces B: Biointerfaces, **2009**, 68, 55-60.

50. Tréguer-Delapierre, M.; Mornet, M.S.; Duguet, E.; Ravaine, S. Synthesis of non-spherical gold nanoparticles. Gold Bulletin, **2008**. 42/2, 195-207.

51. Guo, Z.; Fan, L.; liu, L.;Bian, Z.; Gu, C.; Zhang, Y.; Gu, N.; Yang, D.; Zhang, J. Achieving high-purity colloidal gold nanoprisms and their application as biosensing platforms., Journal of Colloid and Interface Science, 2010, 348;29-36.

52. Kwon, K.; Lee, K.Y.; Lee, Y.K.; Kim, M.; Heo,J.; Ahn, S.J.; Han, S.W. Controlled Synthesis of Icosahedral Gold Nanoparticles and Their Surface-Enhanced Raman Scattering Property. J.Phys. Chem. C 2007, 111, 1161-1165.

53. Allpress, J.G.; Sanders, J.V. The structure and orientation of crystals in deposits of metals on mica, Surf. Sc. **1967**, 7, 1-25.

54. Bukhari, S.B.; Memon, S.; Mahroof-Tahir, M.; Bhanger, M.I. Synthesis, characterization and antioxidant activity copper-quercetin complex. Spectrochimica Acta, **2009**, A 71, 1901-1906

55. De Souza, R. F. V.; De Giovani, W. F. Redox Rep, 2004, 9: 97

56. Jovanovic, S. V.; Steeken, S.; Tosic, M.; Marjanovic, B.; Simic, M.G. J. Am. Soc. 1994, 116: 4846.

57. Nirmala, G.A.;Pandian, K. Antibacterial efficacy of aminoglycosidic antibiotics protected gold nanoparticles- a brief study. Collo. Surfa A. Physicochem Eng Aspects, **2007**, 297:63

58. Zawrah, M.F.; Sherein, I. Antibacterial activities of gold nanoparticles against major foodborne pathogens. Life Sci J, **2011**, 8:37.